OPTIMIZATION OF THE QWITT DIODE USING EQUIVALENT CIRCUIT MODELS

M.J. Paulus+, D.W. Whitson†, C.E. Stutz, K.R. Evans*, E. T. Koenig and R. Neidhard

Electronic Technology Laboratory, Wright Research and Development Center, Wright-Patterson AFB, OH 45433-6543

ABSTRACT

We experimentally investigate an equivalent circuit and an equivalent circuit/distributed impedance model for the QWITT diode. Both models incorporate a negative inductor to model the finite lifetime of carriers in the quantum well. For the latter model one can optimize the cut-off frequency and the negative resistance with respect to the drift region length, W. It is predicted and experimentally confirmed at low values of W that the cut-off frequency increases with W. The two models diverge as W increases and the drift angle is found to be a good predictor for this behavior.

INTRODUCTION

Quantum well diodes (QWD's) can be used as high frequency r.f. sources, (e.g. 420 GHz Sollner et. al. (1)), but are normally limited to micro-watt power levels. With the quantum well injection transient time (QWITT) diode (2), the addition of a drift region increases the magnitude of the total negative resistance and subsequently the power capability of the device. An accurate small signal model is needed in order to design a device with optimized cut-off frequency (f_{co}) and negative resistance magnitude. We have validated an equivalent circuit model for the QWD and propose a modified equivalent circuit/distributed impedance model for the QWITT. Model predictions are compared with experimental data for five double barrier structures with different drift region lengths (W). In addition, devices recently reported in the literature are analyzed using the two models.

The following new results are obtained:

- The use of a negative inductor (3) to model the delay due to the lifetime of the quasi-bound state is verified.
- For devices with 5nm-5nm-5nm AlGaAs-GaAs-AlGaAs double barrier structures, the magnitude of the negative resistance and cut-off frequency are found to increase as the drift region length is increased.
- The two models (QWD and QWITT) are found to be equally accurate for the 5nm-5nm-5nm AlGaAs-GaAs-AlGaAs double barrier structures studied here. However, if the drift region delay is greater than the lifetime of carriers in the quantum well quasi-bound states, the QWITT model must be used.
- The best predictor of agreement between the QWD and QWITT models is shown to be the calculated drift angle (θ_d).
- It is possible to optimize the cut-off frequency and the magnitude of the negative resistance by appropriate choice of the drift region length.

SMALL SIGNAL MODELS

The QWD small signal model employed here is similar to the equivalent circuit recently proposed by Brown et. al.(3). Shown in Figure 1a, their model differs from previous models by the inclusion of a negative inductance (L_{q1}) to model the current delay due to the finite lifetime of the quasibound state (τ_q), where $L_{q1} = \tau_q R_{q1}$ and R_{q1} is the negative resistance of the device. Under this model, the electrical characteristics of the drift region are incorporated into the equivalent circuit components. For example, the QWD capacitance (C_{q1}) includes both the double barrier structure and the drift region. The effect of increasing the drift region length is to decrease C_{q1} and increase the magnitude of R_{q1}.

The QWITT model treats the drift region as a separate distributed impedance. Our QWITT model is shown in Figure 1b, where the inclusion of L_{q2} distinguishes it from previous models (2). The drift region depends on the injector equivalent circuit parameters by the following relationship:

(1)

$$Z_{tt}(\omega) = \frac{v_s((1-\omega^2 L_{q2}C_{q2})(1-\cos\theta_d)+\omega R_{q2}C_{q2}\sin\theta_d)}{\omega^2 \varepsilon_2 A((\omega R_{q2}C_{q2})^2+(1-\omega^2 L_{q2}C_{q2})^2)}$$

$$-j\frac{w}{\omega\varepsilon_2 A}\left(1+\frac{\omega R_{q2}C_{q2}(1-\cos\theta_d)-(1-\omega^2 L_{q2}C_{q2})\sin\theta_d}{\theta_d((\omega R_{q2}C_{q2})^2+(1-\omega^2 L_{q2}C_{q2})^2)}\right)$$

In the injector equivalent circuit, $L_{q2} = \tau_q R_{q2}$ where R_{q2} is the negative resistance contribution due only to the quantum well and its barriers.

The capacitance in the QWITT model injector (C_{q2}) is calculated from barrier to barrier length. The effect of increasing the drift region length is described by Eqn. 1.

At low frequencies the total negative resistance of the QWD model reduces to $R_s + R_{q1}$ and that for the QWITT model to $R_s + R_{q2} + Re(Z_{tt})$. If we equate these expressions, we have

$$(2) \quad R_{q1} \approx R_{q2} \{ 1 + (W/D_{eff})[1 + W/(2v_S R_{q2} C_{q2})] \}.$$

or

$$(3) \quad R_{q2} = [R_{q1} - W^2 /(\varepsilon_2 A v_S)]/(1 + W/D_{eff}).$$

In Eqns. 2 and 3, Deff is the electrical length of the barriers and well and ε_2 is the dielectric constant of the drift region. From these equations, the value of R_{q2} can be calculated from an experimentally obtained value for R_{q1} and the device geometry. Once R_{q2} is known for a given W, R_{q1} can be calculated for all values of W.

EXPERIMENTAL PROCEDURE

The five samples studied here were grown in a Varian 360 MBE system. A schematic diagram of the MBE structures is shown in Figure 2. The samples are identical except for layer 8 which has thicknesses of 20nm (H91), 50nm (H87), 100nm (H88), 150nm (H89) and 200nm (H90).

The devices were r.f. characterized at room temperature using an HP8510B Automated Network Analyzer with Cascade Microtech probes. Impedance parameters were obtained from devices biased in their NDR regions over the frequency range 0.045-26.5 GHz and fit to the QWD and QWITT models using a modified Levenberg-Marquardt least squares routine. The extracted model parameters are given in Table I. R_{s1} is process dependent and found to vary among the samples. As expected, C_{q2} decreases and, in general, R_{q1} increases with increasing drift length. R_{q1} and L_{q1} are strongly bias dependent, but their ratio, $\tau_q = L_{q1}/R_{q1}$ is relatively constant for all five samples. The extracted QWITT model drift lengths indicate the $2X10^{16}$ layers which are longer than 50nm do not fully deplete when the devices are biased in their NDR regions.

To demonstrate the importance of including the negative inductor in the QWD and QWITT models, we plotted measured impedances and best fit curves for H89A using the QWD model with and without L_{q1} (Fig. 3). Across the entire frequency range, the fit to experimental data is greatly improved by the inclusion of L_{q1} in the equivalent circuit.

The absolute value of the total resistance vs. frequency is plotted in Fig. 4 for H91A, H87A and H89A. At virtually every frequency, the magnitude of the negative resistance is greater for devices with longer drift lengths. Furthermore, the 3dB roll-off point and f_{co} occur at higher frequencies for devices with longer drift lengths. Therefore, for these devices, the power output and frequency range should both improve with increasing W. The measured f_{co} vs. W is shown in Fig. 5 along with the predictions of the QWD and QWITT models. For these devices, the QWD and QWITT models are in close agreement with one another and with the experimental data.

It is evident from Fig. 5, however, that the QWD and QWITT models do diverge at higher frequencies. To investigate the differences between the QWD and QWITT models, we analyzed the very high frequency RTD oscillators reported by Sollner et. al. (4). The devices described in Ref. 4 differ from H87-H91 in that the delay due to the finite quasi-bound state lifetime is extremely short ($\tau_q < 5$ ps). As a result, the delay due to even a short drift region can be significant, and the QWITT model must be used to describe that delay. Material parameters for these devices were taken from Table I of Ref. 4 and are summarized in Table II. Drift regions are formed in these devices by the depletion of the doped layers outside the double barrier structure. The QWD and QWITT equivalent circuit parameters are given in Table III. Using these device parameters, values of f_{co2} (cut-off frequency for the QWITT model) and f_{co1} (cut-off frequency for the QWD model) were calculated as a function of W for Dev. #3 ($\tau_q \approx 0.4$ ps). As shown in Fig. 6, the QWD model becomes inaccurate for depletion widths greater than approximately 20 nm. For example, at W=300 nm the QWD model predicts a cutoff frequency of 900 GHz. Yet, the transit delay for the drift region alone would be approximately 3 ps, which would correspond to a cut-off frequency of only 53 GHz. The best predictor of the level of agreement between the QWD and QWITT model is found to be the drift angle of the depletion region. For example, if $\theta_d < 10°$, the models will agree within approximately 5%. If $\theta_d < 3°$, the models will agree within approximately 1%.

Using the QWITT model, it is possible to calculate the drift length required to optimize f_{co}. Table IV compares the experimental values of the drift length and f_{co} with calculated optimum values. For all the devices except Dev #3, W should have been longer. Dev. #3 is near its optimum W and has a reported cutoff frequency of 201 GHz.

The authors express their sincere gratitude to J.E. Ehret, C.I. Isbill, B.J. Johnson, D. Mays, J.R. Roesner, R. Scherer, E.N. Taylor, and G. Wilder for their technical support and to G.L. McCoy, R. Walline, K. Soda, and C.I. Huang for fruitful discussions. One of the authors (DWW) was supported under the AFOSR Resident Research Program and is now at Indiana University of Pennsylvania. Another author (KRE) is supported under USAF Contract F33615-86-C-1050. Another author (MJP) is now at the Georgia Tech Microelectronics Research Center.

(1) E.R. Brown, T.C.L.G. Sollner, C.D. Parker, W.D. Goodhue, and C.L. Chen, Appl. Phys. Lett., 55(7), 1777 (1989).
(2) V.P. Kesan, D.P. Neikirk, P.A. Blakey, B.G.Streetman, and T.D. Linton, Jr., IEEE Trans. Elec. Dev., 35(4), 405 (1988).
(3) E.R. Brown, C.D. Parker, T.C.L.G. Sollner, Appl. Phys. Lett., 54(10), 934 (1989).
(4) T.C.L.G. Sollner, E.R. Brown and H.Q. Lee, Lincoln Lab Jou., 1(1), 89-106 (1988).

Table I. Fitted QWD and QWITT equivalent circuit parameters. H88 was processed separately.

QWD Model

	H91	H87	H88*	H89	H90
R_S (Ω)	10.2±.2	9.3±.3	3.4±.1	5.3±.3	9.1±.3
C_{Q1}(fF)	370 ± 3.	208 ± 1.	138±.4	115 ± .5	98.8±.2
R_{Q1} (Ω)	-105 ± .8	-113 ± .6	-392±.8	-153 ± .6	-383±.7
L_{Q1} (nH)	-3.42 ± .07	-1.72 ± .04	-4.84±.09	-2.75 ± .03	-4.56±.06
τ_q (ps)	32.5	15.2	12.3	17.9	11.9

Qwitt Model

R_S (Ω)	11.0±.1	10.7±0.2	2.3±.1	5.1±.2	8.0±.2
C_{Q2} (fF) calc.	877	877	877	877	877
R_{Q2} (Ω)	-43.3 ± .4	-28.1 ± .2	-61.9±.2	-21.5 ± .1	-43.4±.1
L_{Q2} (nH)	-1.12 ± .02	-.34 ± .01	-.81±.01	-.38 ± .01	-.523±.004
W (nm)	23.9 ± .2	53.3 ± .2	88.5±1.5	110 ± .5	131±.2

Table II: Summary of material parameters from Table I of Ref. 4.

Barrier material	Dev # 1 AlAs	Dev # 2 AlGaAs	Dev # 3 AlAs (x=0.3)
Barrier thickness (nm)	2.5	3.0	1.5
Well thickness (nm)	4.5	4.5	4.5
Doping outside barriers	1e18	2e17	2e17
Diameter (microns)	4.0	4.0	4.0
Quasibound state lifetime (ps)	4.0	0.16	0.4
Drift length			Field dependent

Table III: Estimated equivalent circuit parameters for samples reported in Ref. 4.

QWD Model

	Dev #1	Dev #2	Dev #3
R_S (Ω)	35.7	42.4	4.24
C_{Q1}(fF)	56.1	35.5	18.6
R_{Q1} (Ω)	-200	-125	-77
L_{Q1} (nH)	-0.80	-0.020	-0.031

Qwitt Model

R_S (Ω)	35.7	42.4	4.24
C_{Q2} (fF) (calculated)	133	132	174
R_{Q2} (Ω)	-100	-46	-10.9
L_{Q2} (pH)	-400	-7.36	-4.36
W (nm)	15	30	70

Table IV: Comparison of experimental and optimum f_{CO} vs W. ‡150 μm² mesas.

*Data from Table I of Ref. 4.

	W(extracted) (nm)	fco(exp.) (GHz)	W(optimum) (nm)	fco(max) (GHz)
H91A‡	27.1	6.25	271	19.0
H87A‡	67	10.5	271	19.0
H89A‡	127	17.4	271	19.0
Dev #1*	15	20.7	213	40.4
Dev #2*	30	43.7	188	83.2
Dev #3*	70	201	53.3	206

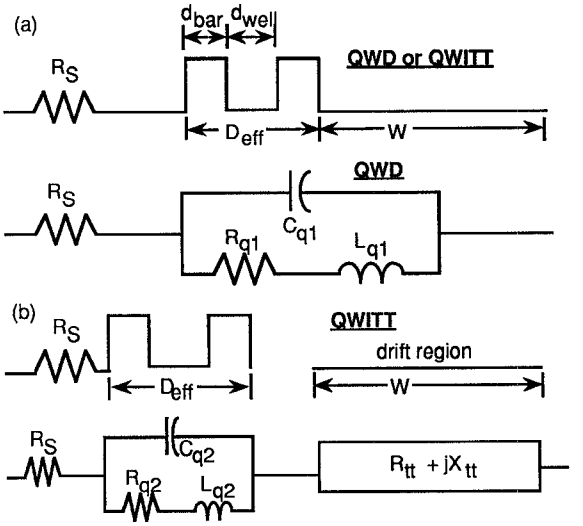

Fig. 1(a). QWD equivalent circuit model. The double barrier structure and drift region characteristics are both included in the lumped impedance model. (b) QWITT equivalent circuit/distributed impedance model. The double barrier injector is modeled by the lumped impedance model and the drift region is modeled by the distributed impedance Z_{tt}.

Layer 1	300 nm	5 x 10^{18}	n - GaAs
Layer 2	50.0 nm	2 x 10^{16}	n - GaAs
Layer 3	2.5 nm	UD	GaAs
Layer 4	5.1 nm	UD(x=.42)	AlGaAs
Layer 5	5.1 nm	UD	GaAs
Layer 6	5.1 nm	UD(x=.42)	AlGaAs
Layer 7	2.5 nm	UD	GaAs
Layer 8	L	2 x 10^{16}	n - GaAs
Layer 9	700 nm	5 x 10^{18}	n - GaAs

Fig.2.MBE layers: L(H91)=20 nm; L(H87)=50 nm; L(H88)=100 nm;L(H89)=150 nm;L(H90)=200 nm

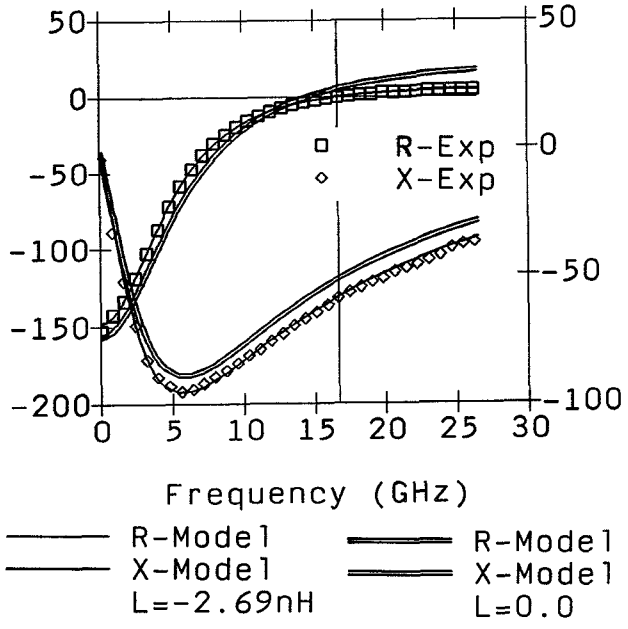

Fig. 3. Left vertical axis is resistance (Ohms) and the right vertical axis is reactance (Ohms). Comparison of best fits for the QWD model with (single line) and without (double line) the negative inductance L_{q1} for a 150 μm^2 mesa on sample H89. Best fit values without L_{q1} are R_{s1} = 26.3Ω, C_{q1} = 0.144 pF and R_{q1} = -183Ω. Best fit values with L_{q1} are L_{q1} = -2.69 nH, R_{s1} = 6.03Ω, C_{q1} = 0.118 pF and R_{q1} = -154Ω.

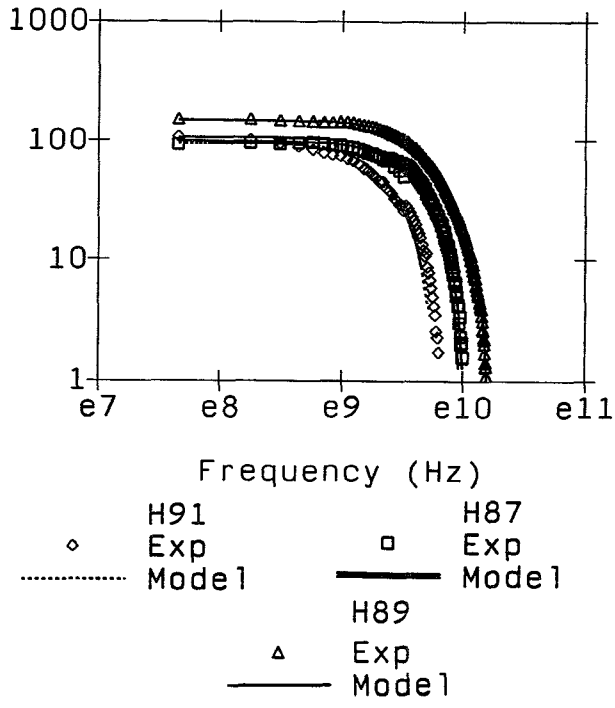

Fig. 4. The absolute value of the measured resistance in Ohms (vertical axis) vs. frequency for 150 μm^2 mesas.

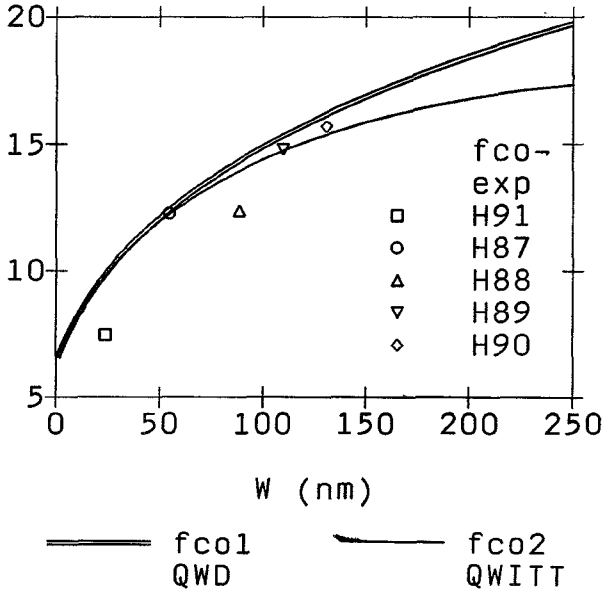

Fig. 5. The vertical axis is fco in GHz. Measured f_{co} (normalized to R_s = 8.0Ω) for samples H91, H87, H88, H89, and H90. Predicted f_{co} vs frequency for the QWD (f_{co1}, double line) and QWITT (f_{co2}, single line) models based on the extracted parameters of H89 are also shown.

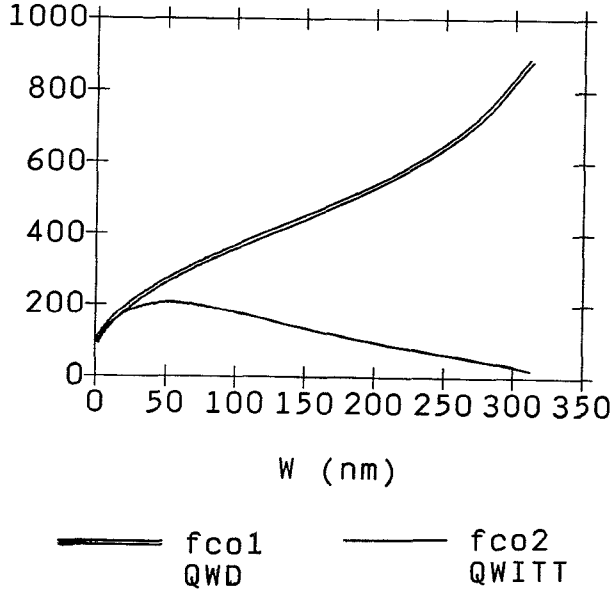

Fig. 6. The vertical axis is the cut-off frequency, fco, in GHz. Comparison of QWD (double line; f_{co1}) and QWITT (single line; f_{co2}) model predictions for Sample #3 of Ref. 4.